Supplementary Material: Characterising Experimental Alluvial Fan Dynamics Using Dense Optical Flow and DEMs of Difference

Nastaran Nematollahi[1, 2], Brett Eaton[1, 2], and Sarah Davidson[1, 2]

[1]Department of Geography, University of British Columbia, 1984 West Mall, Vancouver, BC V6T 1Z2, Canada
[2]BGC Engineering Inc., 980 Howe Street, Vancouver, BC V6Z 0C8, Canada

Correspondence: Nastaran Nematollahi (nasipour@student.ubc.ca)

1 Supplementary Methods: Detailed Description

Here we provide additional details about the equipment, data sources, and preprocessing steps used in the experiment. Specifically, we describe the camera setup, the two datasets collected (3D photogrammetry images and high-frequency RGB images), and the methods applied to prepare these datasets for analysis.

S1.1 Equipment

A total of seven Canon EOS Rebel T6i DSLRs were used in the experiment. One camera was mounted directly overhead, 1.5 m above the center of the fan surface, oriented vertically downward, and captured RGB images at 3-second intervals to document surface flow patterns at high spatial and temporal resolution. The remaining six cameras were dedicated to Structure-from-Motion (SfM) photogrammetry for generating digital elevation models (DEMs). These cameras were mounted side-by-side on a rigid rail system positioned 1.0 m above the fan table. The rail was moved in 10 cm increments along the 2.5 m table length, and at each stop all six cameras were triggered simultaneously, producing 78 photographs per DEM acquisition. Based on the APS-C sensor size (22.3 × 14.9 mm), focal length of 18 mm, and camera height of 1.0 m, each image covered a ground footprint of ~1.2 × 0.8 m, yielding a ground sampling distance of ~0.24 mm/pixel and forward overlap of 88–92%. Photogrammetry image sets were collected every 30 minutes, after water flow had stopped and the fan surface had drained, ensuring a static, reflection-free bed. Camera positions are shown in the main manuscript (fig.1).

We conducted photogrammetry in Agisoft Photoscan Professional (Version 1.4.5, build 7354). The image sets were processed using high-quality settings for image alignment and aggressive filtering to generate dense topographic point clouds.Each dense cloud contained over 11 million points, yielding an average density of approximately 3.4 million points per square meter, equivalent to a mean point spacing of ~0.55 mm. From these point clouds, we produced DEMs at 0.5 $mm/pixel$ resolution.

All cameras were identical Canon EOS Rebel T6i DSLRs equipped with Canon EF-S 18–55 mm lenses fixed at 18 mm focal length. They were set to an aperture of f/10 and ISO 400, with focus adjusted manually before each experiment and autofocus disabled to maintain consistency. Illumination was provided by two LED lights positioned at the downstream corners, while

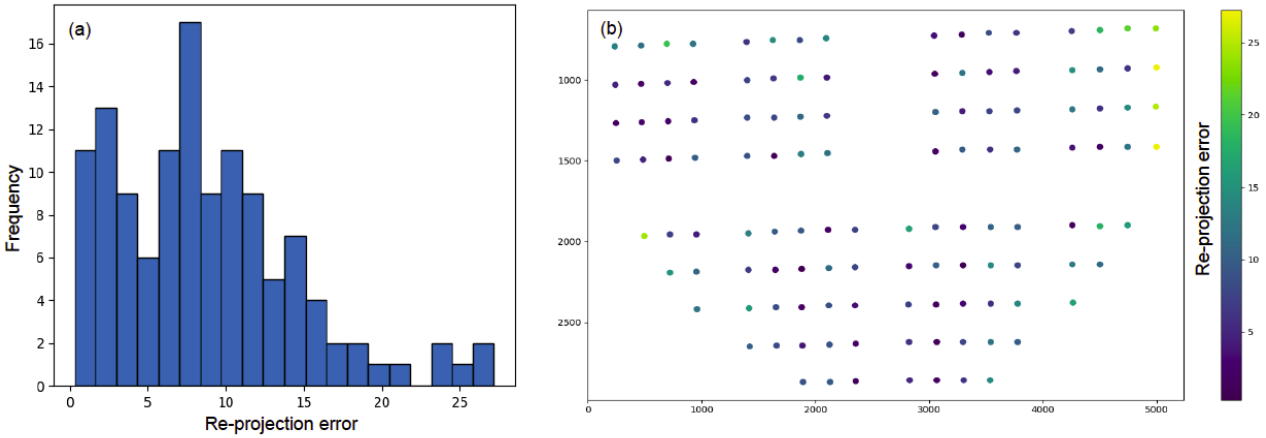

Figure S1. Distribution of re-projection errors following homography-based image transformation.

a translucent plastic sheet covered the setup to reduce glare from ceiling lights and daylight, ensuring uniform lighting and minimal shadowing across image sequences.

S1.2 Image preprocessing

Image preprocessing steps—including georectification, georeferencing, fan surface masking—and optical flow analyses were performed in Python using the OpenCV library (Bradski, 2000). All other analyses, including raster calculations and spatial analysis, were conducted in R using the Terra package (R Core Team, 2025; Hijmans, 2024). All scripts, along with a representative subset of the experimental dataset and animated videos of the experiment, are available in our GitHub repository.

S1.2.1 Image georectification and georeferencing

We corrected the radial distortion of the overhead Canon DSLR camera, which was installed for flow mapping, using Adobe Photoshop's Auto Lens Correction feature, which considers the camera-specific EXIF metadata to apply the appropriate distortion profile. Further, all the rectified images were georeferenced to our defined coordinate system using a reference orthophoto through a homography-based transformation. The accuracy of this alignment was calculated using the mean reprojection error—defined as the Euclidean distance between transformed points in the corrected image and their corresponding locations in the orthophoto—which was 10.11 pixels, equivalent to 10 mm. As shown in Figure 1 (b), the high values of reprojection errors are related to the left and right corners of the image beyond the maximum fan extent. An overlay of the transformed image on the reference orthophoto is presented in Figure 2.

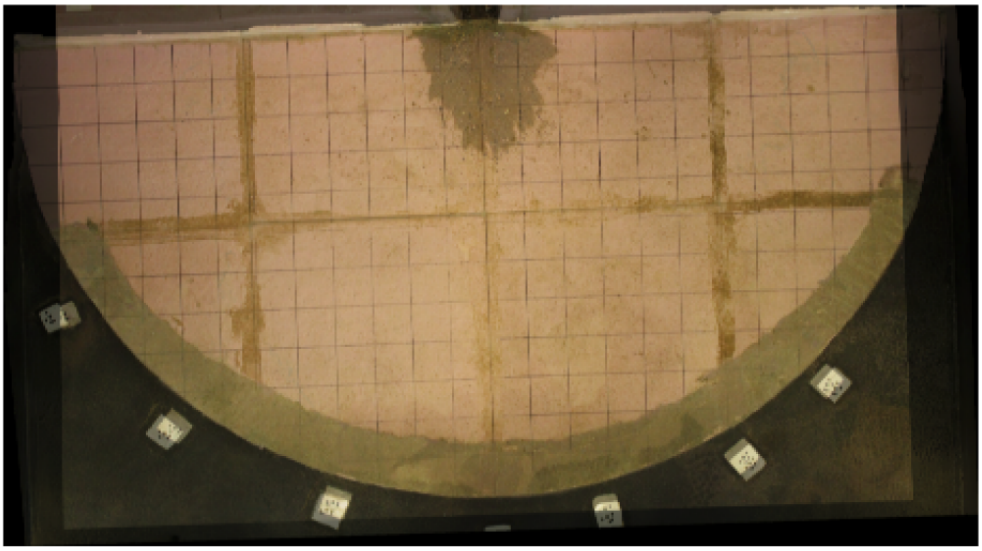

Figure S2. Overlay of orthophoto and transformed image post homography application.

S1.2.2 Fan surface masking

The overhead camera used to capture flow images had a wider field of view than the fan, including parts of the experimental setup and the sheet beneath the fan. To isolate the fan surface, we first applied a Gaussian blur with $\sigma = 5$ to reduce noise caused by grain texture and lighting variability. We then performed intensity thresholding using a value ranging from 112 to 117, which was empirically determined and visually inspected at regular intervals(every 600 images) to account for minor lighting changes over time. We further refined the resulting binary mask using a morphological erosion operation with a 3×3 kernel to eliminate small, isolated noise elements, as shown in Figure 3. The final binary mask was applied to each frame to isolate the active fan surface. These masked images were then used to calculate fan area and fan radius through time and to compile video sequences for optical flow analysis.

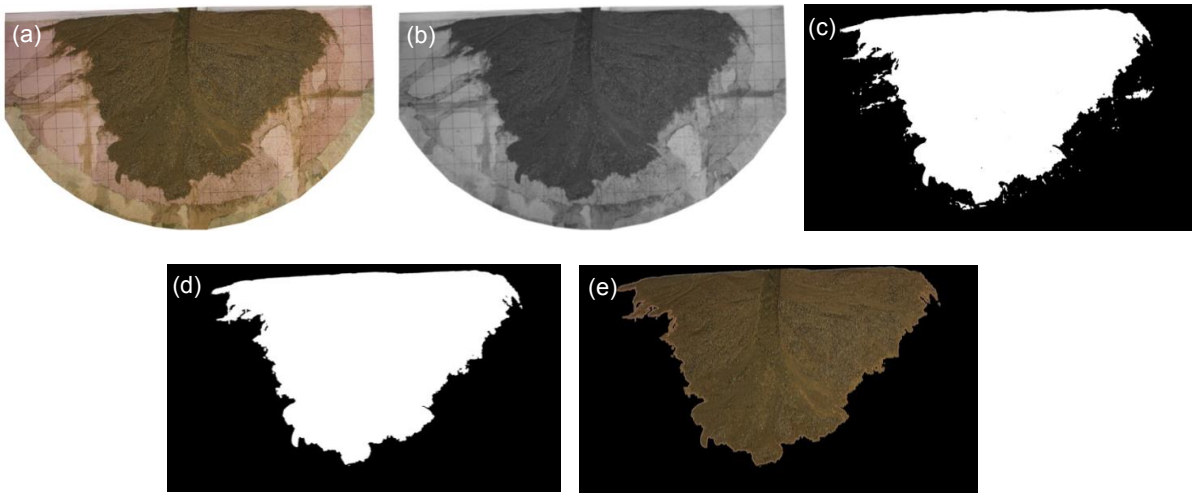

Figure S3. Preprocessing steps for isolating the fan surface. (a) Georeferenced and georectified image. (b) Smoothed image after applying a Gaussian blur filter. (c) Binary mask obtained through intensity-based thresholding. (d) Refined mask following a morphological erosion operation. (e) Final masked fan surface overlaid on the original image.

S1.3 Occupancy maps for all 30-minute analysis windows

The full set of 30-minute occupancy maps is provided here for reference. In each map, pixel values represent the fraction of 1-minute intervals during which that location was classified as active, so the maps show both where activity occurred and how persistently each part of the fan was used. These figures complement the summary metrics in the main text by illustrating the full time series of changes in surface-flow organization.

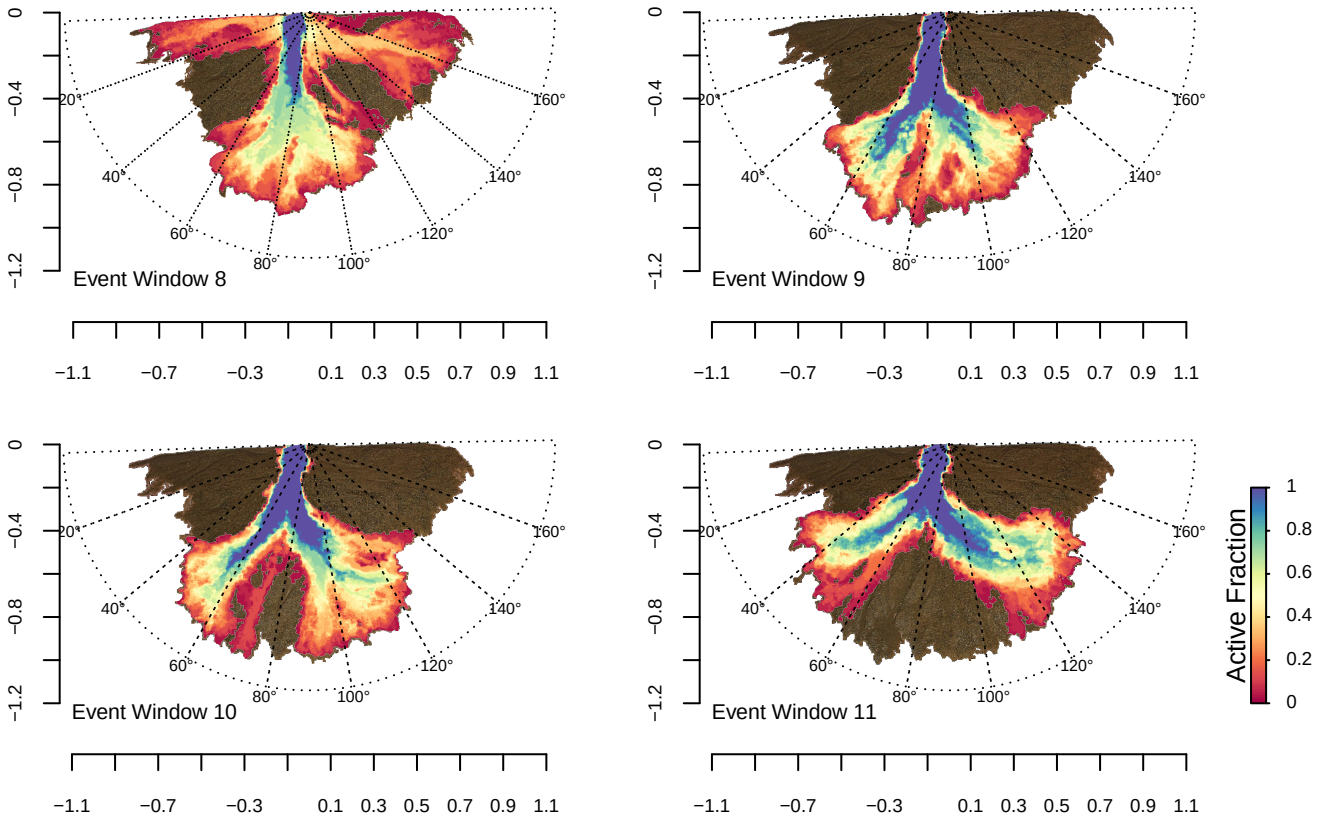

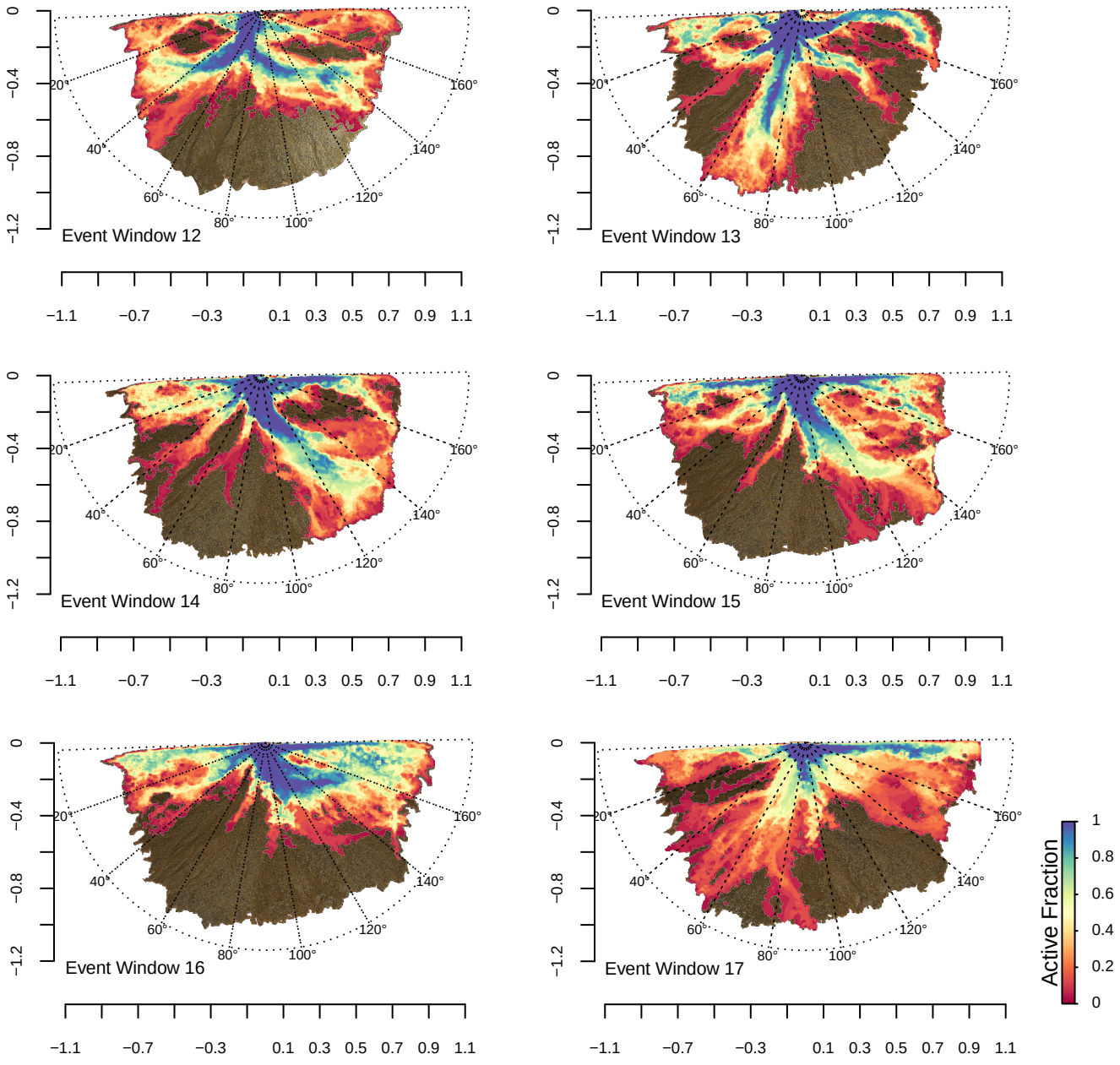
Event Window 12
Event Window 13
Event Window 14
Event Window 15
Event Window 16
Event Window 17
0
−0.4
−0.8
−1.2
20°
40°
60°
80°
100°
120°
140°
160°
−1.1
−0.7
−0.3
0.1
0.3
0.5
0.7
0.9
1.1
Active Fraction
1
0.8
0.6
0.4
0.2
0

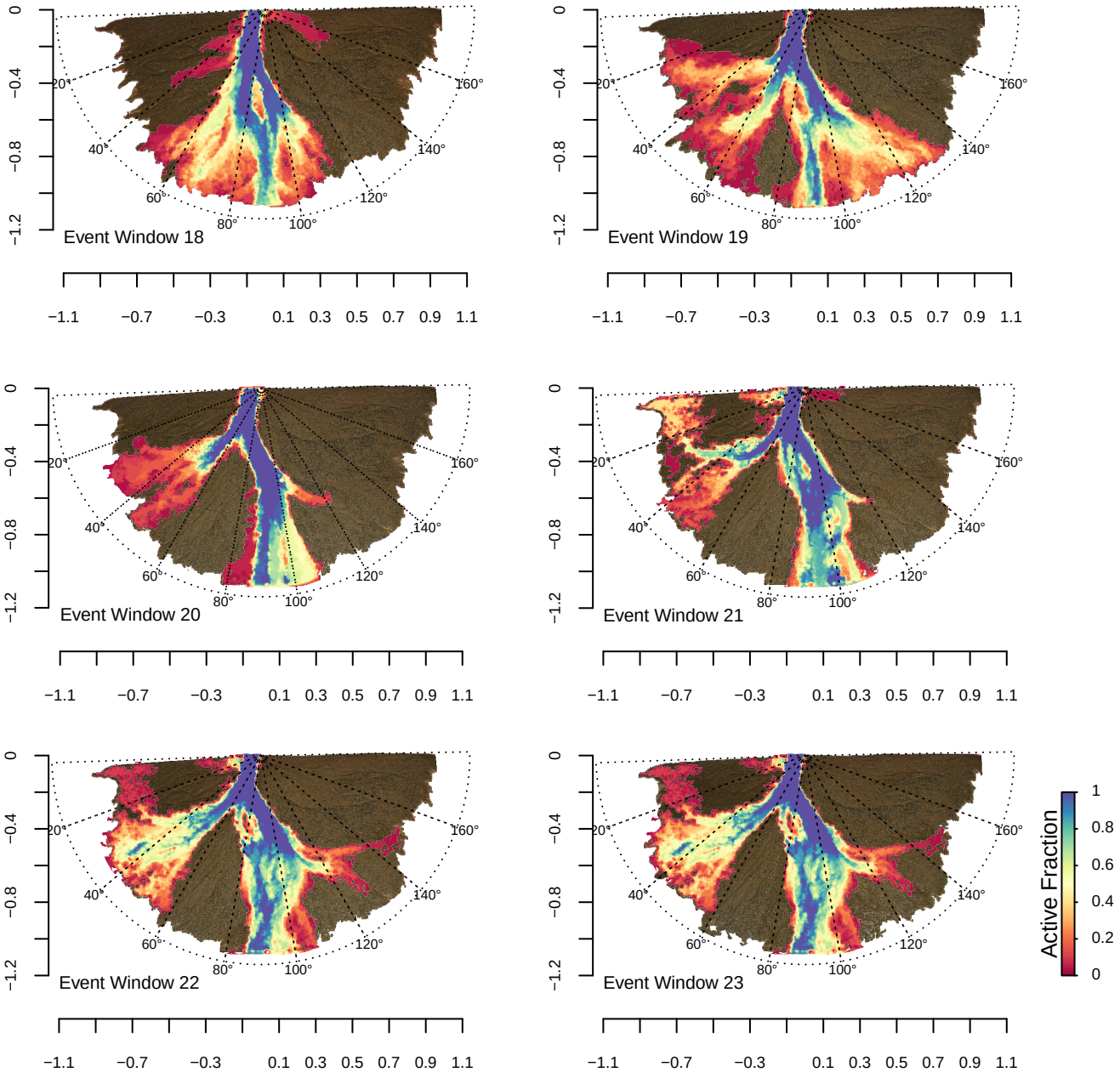
Event Window 18
Event Window 19
Event Window 20
Event Window 21
Event Window 22
Event Window 23
0
−0.4
−0.8
−1.2
20°
40°
60°
80°
100°
120°
140°
160°
−1.1
−0.7
−0.3
0.1
0.3
0.5
0.7
0.9
1.1
Active Fraction
1
0.8
0.6
0.4
0.2
0

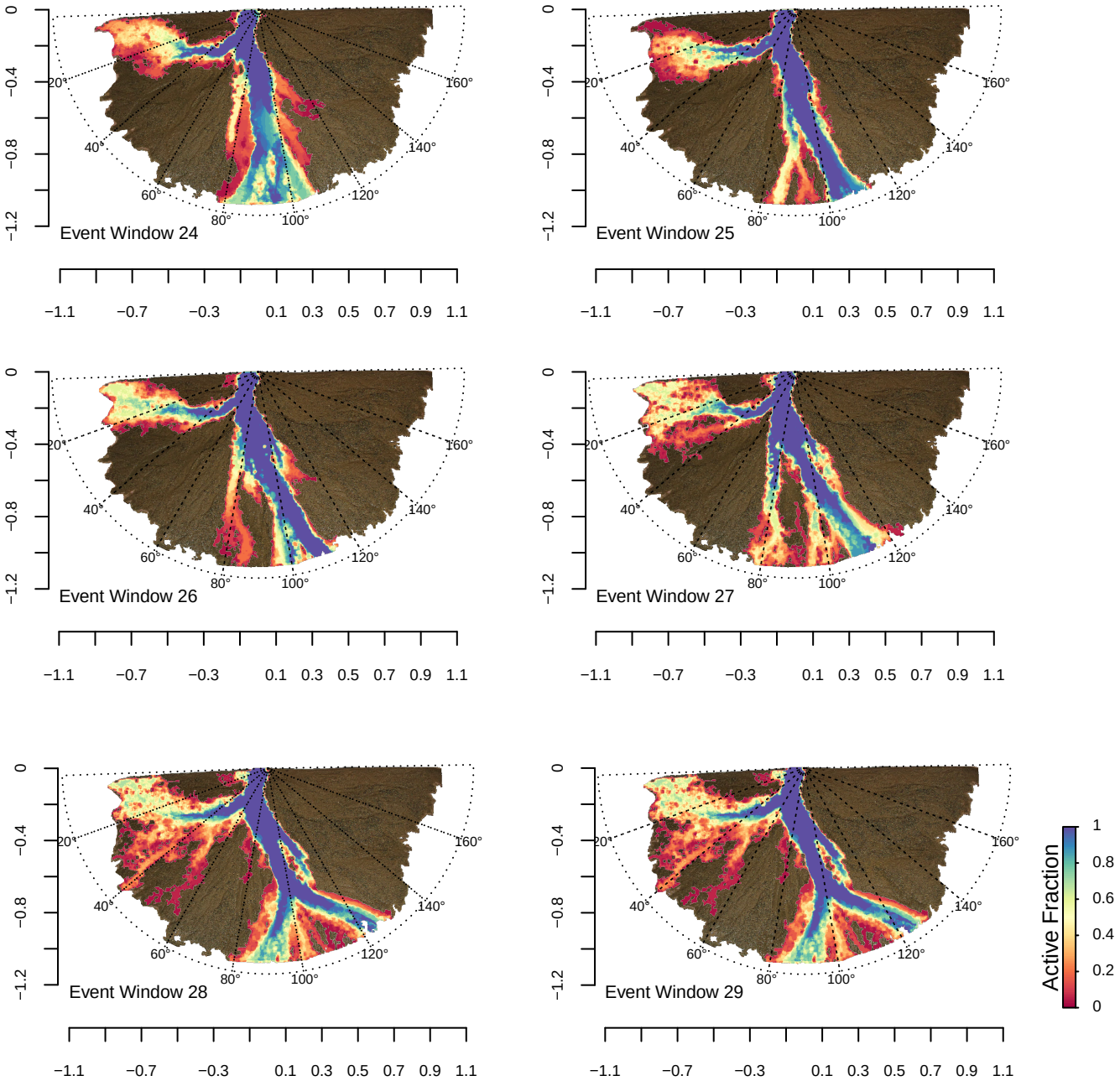
Event Window 24
Event Window 25
Event Window 26
Event Window 27
Event Window 28
Event Window 29
0
−0.4
−0.8
−1.2
20°
40°
60°
80°
100°
120°
140°
160°
−1.1
−0.7
−0.3
0.1
0.3
0.5
0.7
0.9
1.1
Active Fraction
1
0.8
0.6
0.4
0.2
0

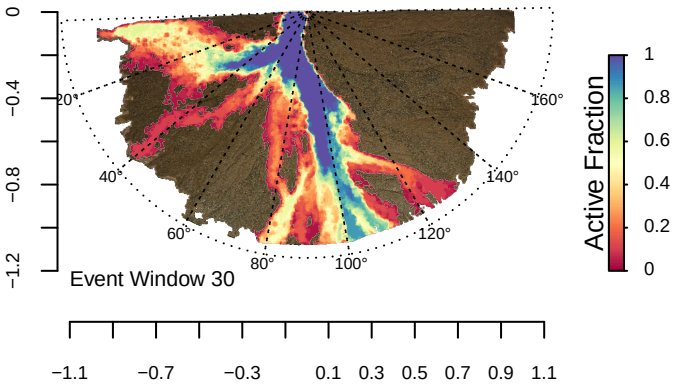

Figure S4. Occupancy maps: colours show the fraction of 1 min intervals during which each pixel was active within each 30 min window.

S1.4 DEMs of Difference for all 30-minute analysis windows

The full set of 30-minute DEMs of Difference (DoDs) is provided here to document the spatial pattern of measurable topographic change throughout the experiment. Each DoD shows net elevation change over a single 30-minute analysis window, with positive values indicating deposition and negative values indicating erosion.

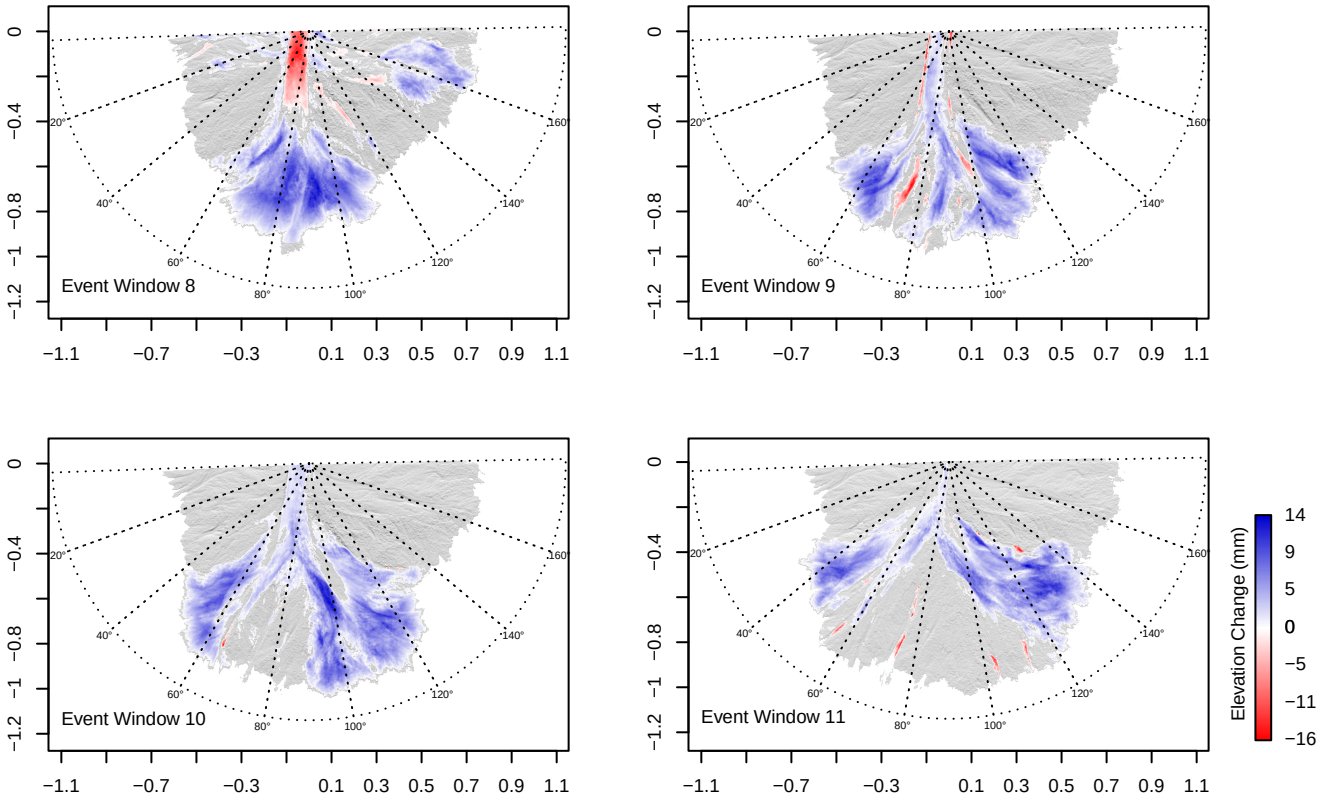

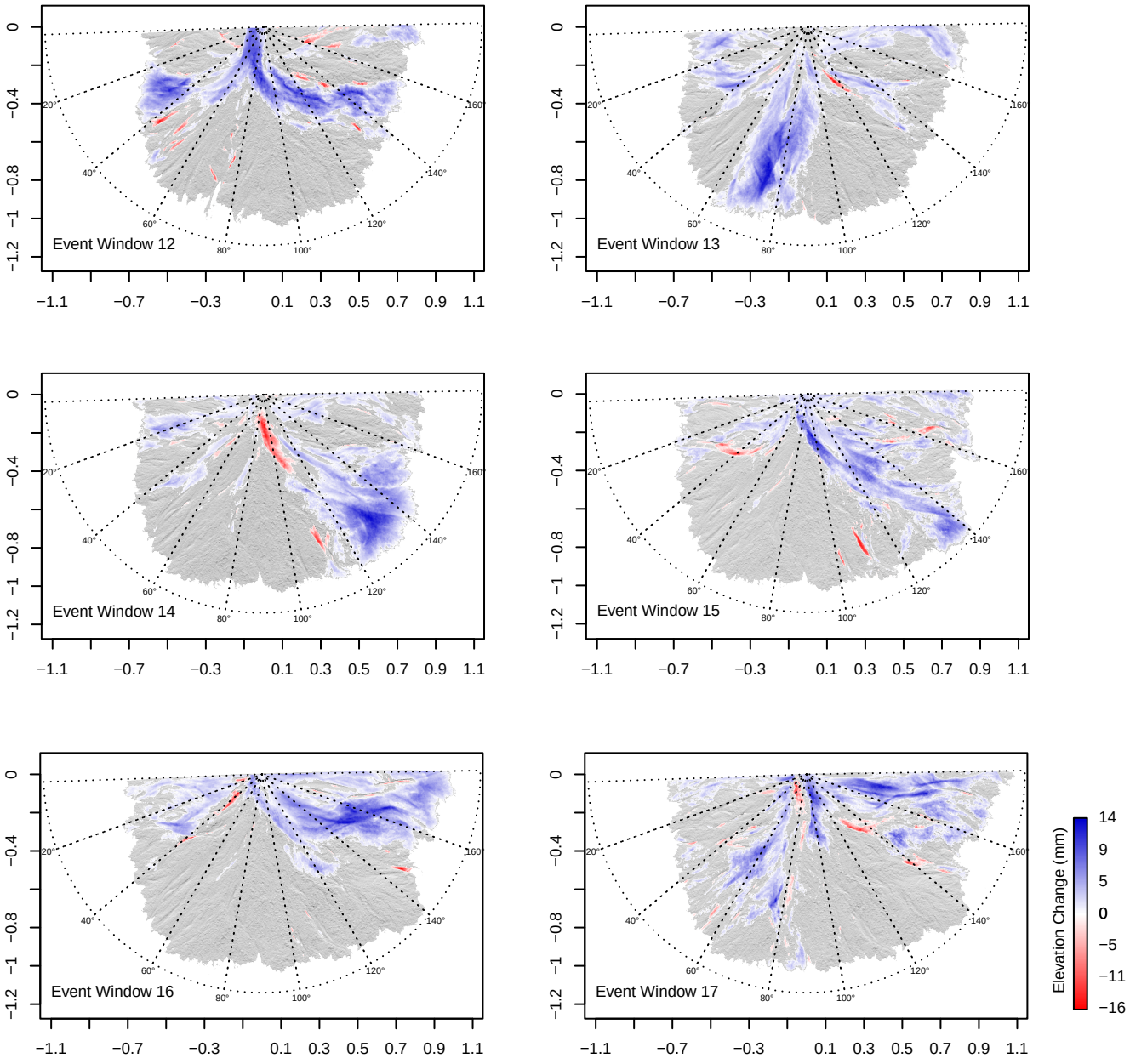
Event Window 12
Event Window 13
Event Window 14
Event Window 15
Event Window 16
Event Window 17
Elevation Change (mm)
14
9
5
0
−5
−11
−16

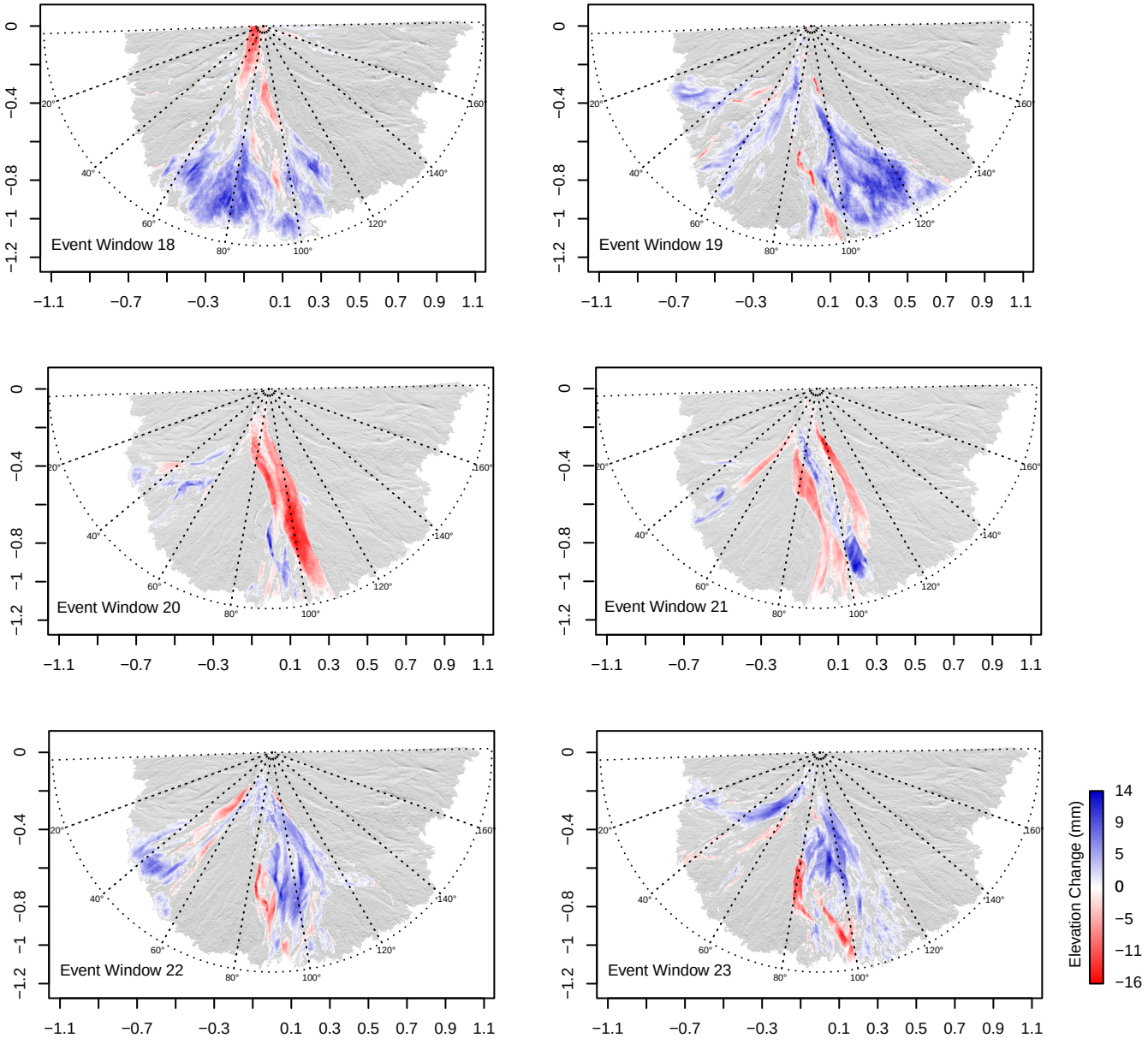
Event Window 18
Event Window 19
Event Window 20
Event Window 21
Event Window 22
Event Window 23
Elevation Change (mm)
14
9
5
0
−5
−11
−16

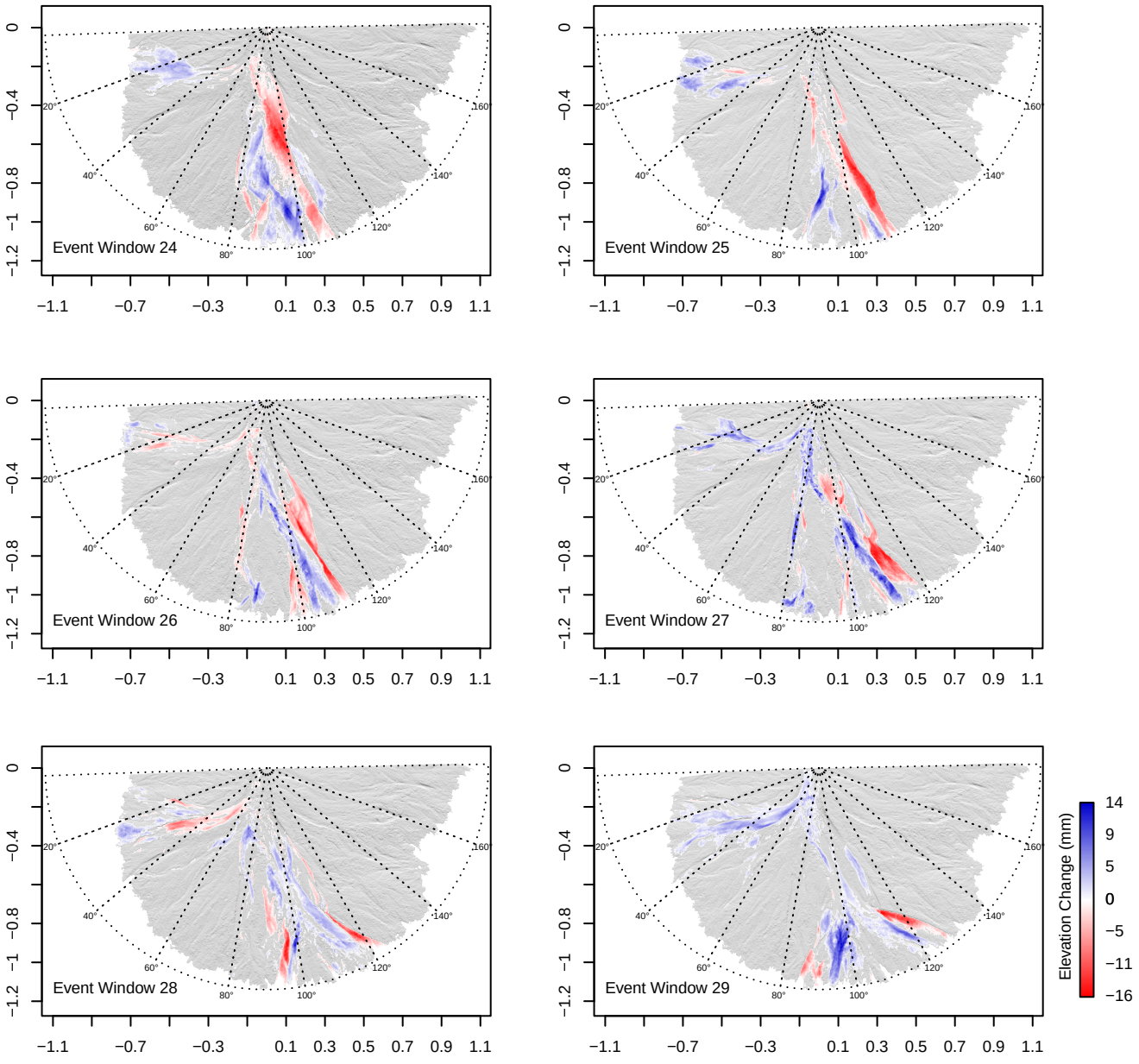
Event Window 24
Event Window 25
Event Window 26
Event Window 27
Event Window 28
Event Window 29
Elevation Change (mm)
14
9
5
0
−5
−11
−16

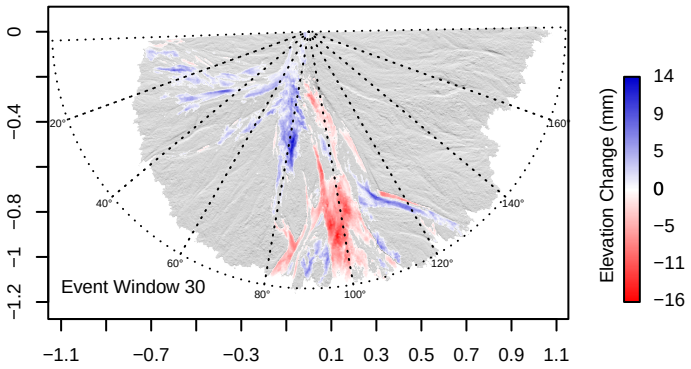

Figure S5. DEMs of Difference (DoDs) for each 30-minute event window. Hillshade is derived from the DEM acquired at the end of each window.

S1.5 Classified overlap maps for all 30-minute analysis windows

The full set of classified overlap maps is provided here to show the spatial agreement between the optical-flow activity maps and the DoD change footprints for each 30-minute analysis window. Each map distinguishes areas detected by both methods, areas detected only by the DoD, and areas detected only by optical flow

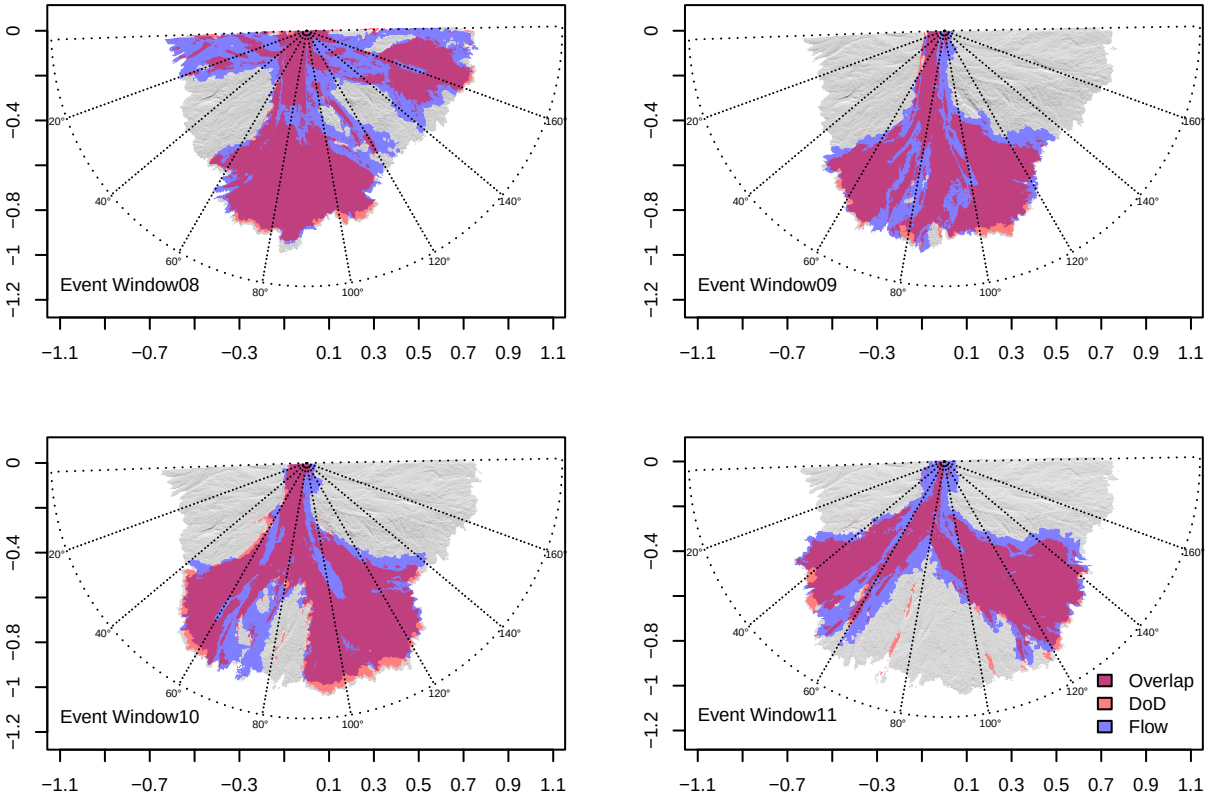

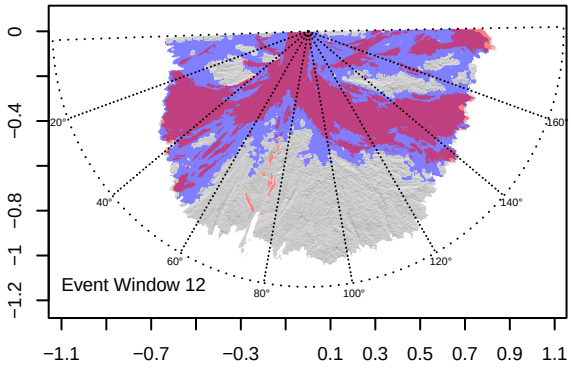
Event Window 12
0
−0.4
−0.8
−1
−1.2
20°
40°
60°
80°
100°
120°
140°
160°
−1.1
−0.7
−0.3
0.1
0.3
0.5
0.7
0.9
1.1

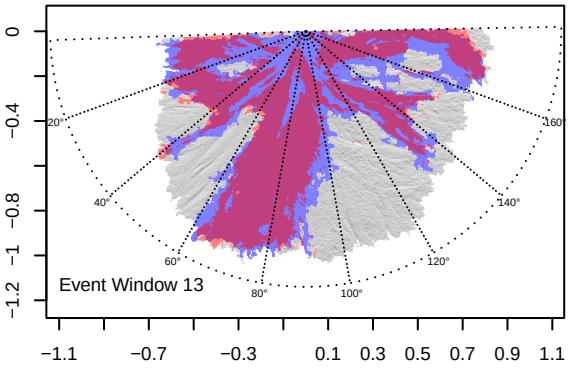
Event Window 13
0
−0.4
−0.8
−1
−1.2
20°
40°
60°
80°
100°
120°
140°
160°
−1.1
−0.7
−0.3
0.1
0.3
0.5
0.7
0.9
1.1

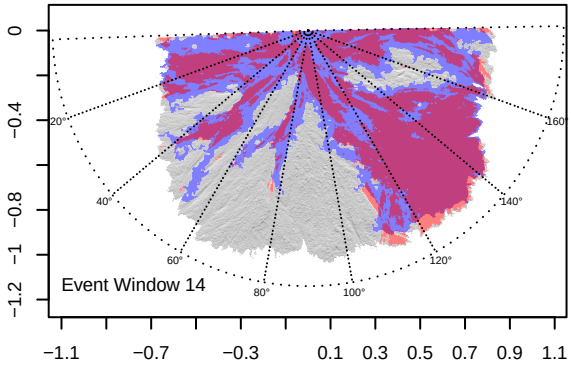
Event Window 14
0
−0.4
−0.8
−1
−1.2
20°
40°
60°
80°
100°
120°
140°
160°
−1.1
−0.7
−0.3
0.1
0.3
0.5
0.7
0.9
1.1

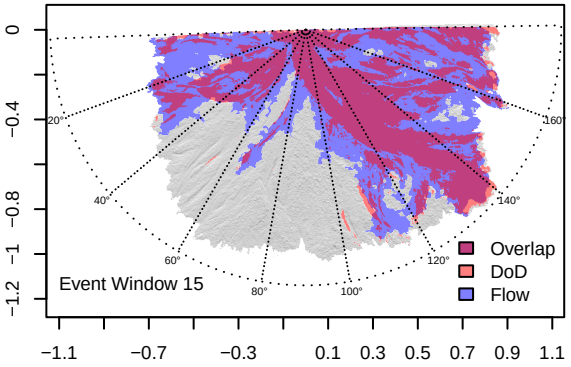
Event Window 15
Overlap
DoD
Flow
0
−0.4
−0.8
−1
−1.2
20°
40°
60°
80°
100°
120°
140°
160°
−1.1
−0.7
−0.3
0.1
0.3
0.5
0.7
0.9
1.1

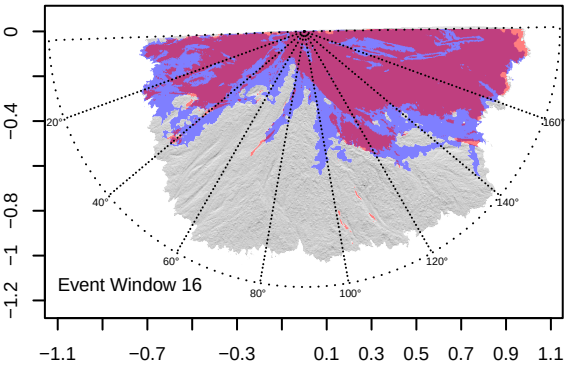
Event Window 16
0
−0.4
−0.8
−1
−1.2
20°
40°
60°
80°
100°
120°
140°
160°
−1.1
−0.7
−0.3
0.1
0.3
0.5
0.7
0.9
1.1

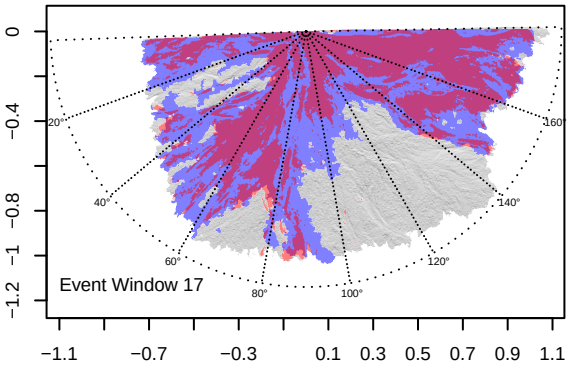
Event Window 17
0
−0.4
−0.8
−1
−1.2
20°
40°
60°
80°
100°
120°
140°
160°
−1.1
−0.7
−0.3
0.1
0.3
0.5
0.7
0.9
1.1

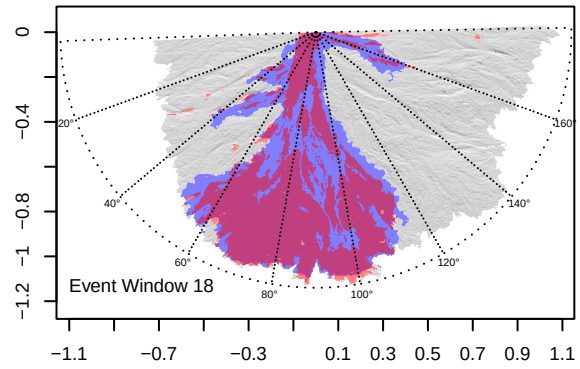
Event Window 18
0
−0.4
−0.8
−1
−1.2
20°
40°
60°
80°
100°
120°
140°
160°
−1.1
−0.7
−0.3
0.1
0.3
0.5
0.7
0.9
1.1

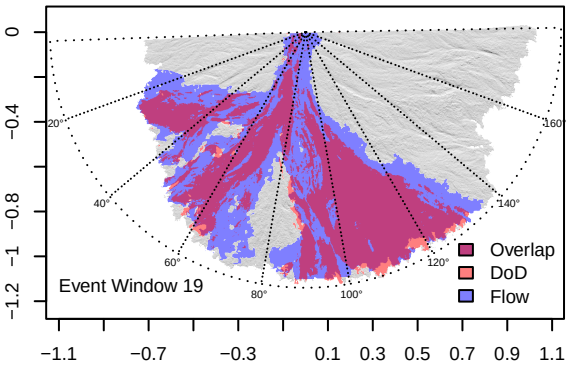
Event Window 19
Overlap
DoD
Flow
0
−0.4
−0.8
−1
−1.2
20°
40°
60°
80°
100°
120°
140°
160°
−1.1
−0.7
−0.3
0.1
0.3
0.5
0.7
0.9
1.1

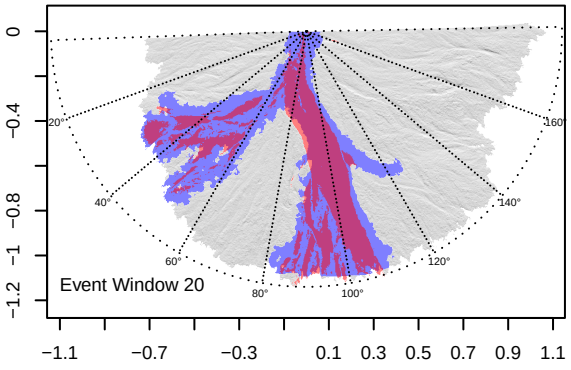
Event Window 20
0
−0.4
−0.8
−1
−1.2
20°
40°
60°
80°
100°
120°
140°
160°
−1.1
−0.7
−0.3
0.1
0.3
0.5
0.7
0.9
1.1

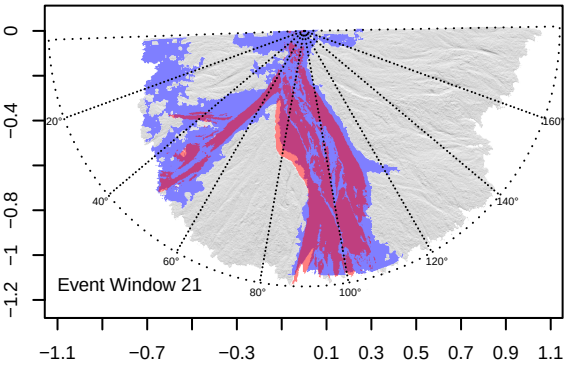
Event Window 21
0
−0.4
−0.8
−1
−1.2
20°
40°
60°
80°
100°
120°
140°
160°
−1.1
−0.7
−0.3
0.1
0.3
0.5
0.7
0.9
1.1

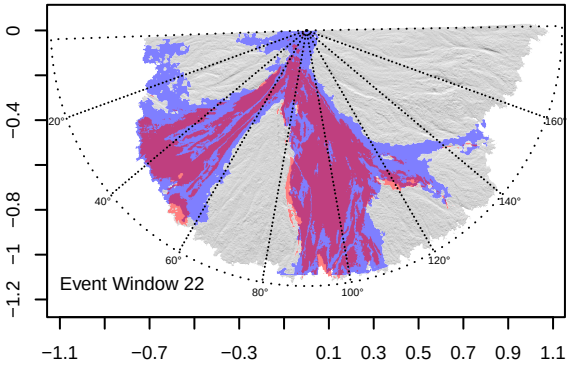
Event Window 22
0
−0.4
−0.8
−1
−1.2
20°
40°
60°
80°
100°
120°
140°
160°
−1.1
−0.7
−0.3
0.1
0.3
0.5
0.7
0.9
1.1

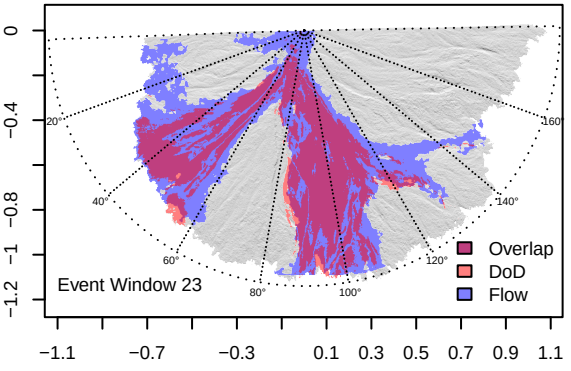
Event Window 23
Overlap
DoD
Flow
0
−0.4
−0.8
−1
−1.2
20°
40°
60°
80°
100°
120°
140°
160°
−1.1
−0.7
−0.3
0.1
0.3
0.5
0.7
0.9
1.1

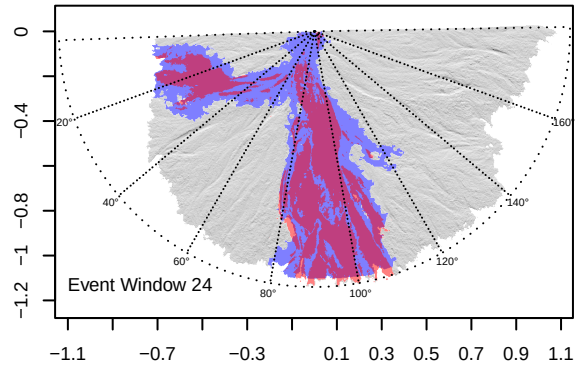
Event Window 24
0
−0.4
−0.8
−1
−1.2
20°
40°
60°
80°
100°
120°
140°
160°
−1.1
−0.7
−0.3
0.1
0.3
0.5
0.7
0.9
1.1

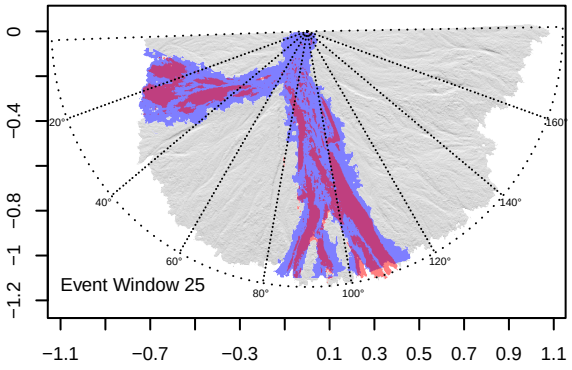
Event Window 25
0
−0.4
−0.8
−1
−1.2
20°
40°
60°
80°
100°
120°
140°
160°
−1.1
−0.7
−0.3
0.1
0.3
0.5
0.7
0.9
1.1

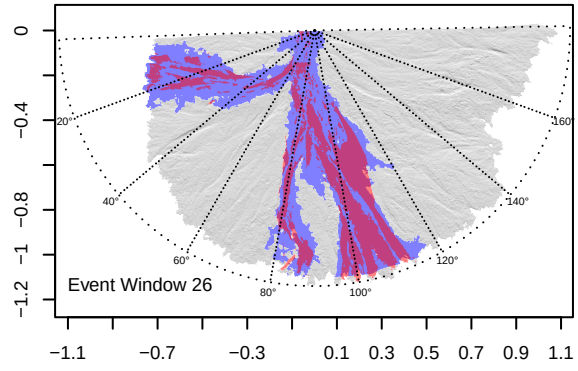
Event Window 26
0
−0.4
−0.8
−1
−1.2
20°
40°
60°
80°
100°
120°
140°
160°
−1.1
−0.7
−0.3
0.1
0.3
0.5
0.7
0.9
1.1

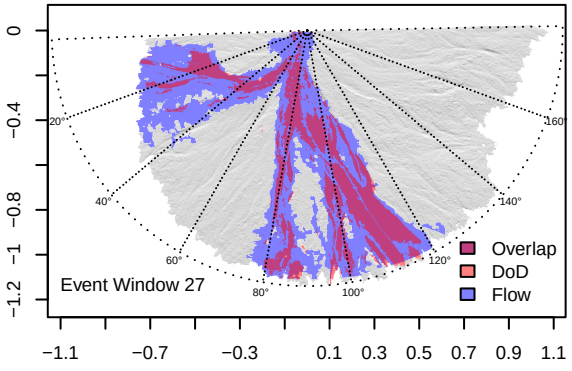
Event Window 27
Overlap
DoD
Flow
0
−0.4
−0.8
−1
−1.2
20°
40°
60°
80°
100°
120°
140°
160°
−1.1
−0.7
−0.3
0.1
0.3
0.5
0.7
0.9
1.1

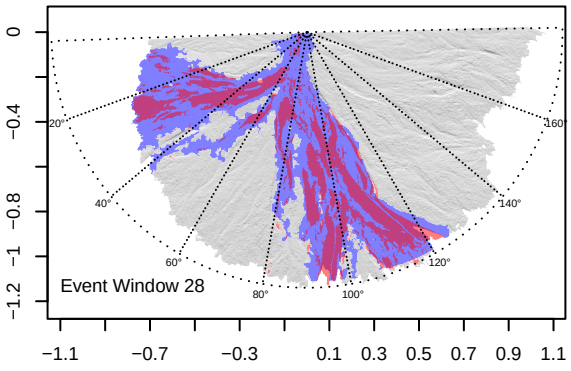
Event Window 28
0
−0.4
−0.8
−1
−1.2
20°
40°
60°
80°
100°
120°
140°
160°
−1.1
−0.7
−0.3
0.1
0.3
0.5
0.7
0.9
1.1

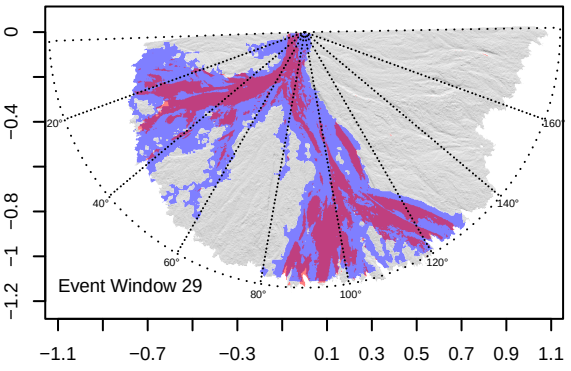
Event Window 29
0
−0.4
−0.8
−1
−1.2
20°
40°
60°
80°
100°
120°
140°
160°
−1.1
−0.7
−0.3
0.1
0.3
0.5
0.7
0.9
1.1

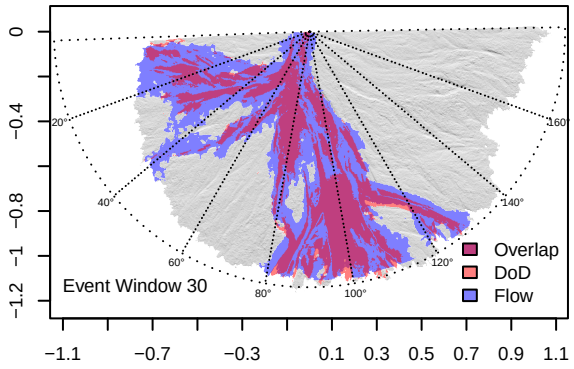

Figure S6. Classified overlap maps comparing the optical-flow activity footprint and the DoD change footprint. Hillshade derived from the DEM acquired at the end of each window.

Code and data availability. The full source data for this study exceed 1 TB in size and are therefore not hosted online. Code and sample data are openly available at: https://github.com/Nastarannmt. The complete datasets are available from the corresponding author upon reasonable request.

Author contributions. NN designed and carried out the experiments, processed optical-flow maps and DEMs, analyzed results, and drafted the manuscript. BRE supervised the study, contributed to interpretation, and edited the manuscript. SD provided technical guidance and contributed to analysis and manuscript revisions.

Competing interests. The authors declare no competing interests.

Disclaimer. The authors used AI-assisted proofreading tools to improve grammar and clarity. All interpretations and conclusions are solely those of the authors.

Acknowledgements. Experimental construction and equipment purchase were supported by an NSERC Discovery Grant awarded to B. Eaton. N. Nematollahi was supported by a Four Year Doctoral Fellowship from the University of British Columbia.

References

Bradski, G.: The OpenCV Library, in: Dr. Dobb's Journal of Software Tools, 2000.

Hijmans, R. J.: terra: Spatial Data Analysis, https://cran.r-project.org/package=terra, r package version 1.7-78, 2024.

R Core Team: R: A Language and Environment for Statistical Computing, R Foundation for Statistical Computing, Vienna, Austria, https://www.R-project.org/, 2025.